Journal of the European Ceramic Society **17** (1997) 61–70
© 1996 Elsevier Science Limited
Printed in Great Britain. All rights reserved
PII: S0955-2219(96)00078-7
0955-2219/97/$17.00

Cyclic Contact Fatigue of CaF_2: Stress Analysis and Experimental Results

C. Maerky, J. L. Henshall, R. M. Hooper & M.-O. Guillou

School of Engineering, University of Exeter, Exeter EX4 4QF, UK

(Received 17 January 1996; revised version received 27 March 1996; accepted 2 April 1996)

Abstract

Surface fatigue is one of the main wear mechanisms in materials, and as such is of considerable relevance to ceramics, which are widely used because of their wear resistance. The purpose of the present study is to develop a general approach to the analysis of plastic-deformation-induced surface fatigue in ceramics. A model material, CaF_2, was chosen since it is isostructural with commercially more important ZrO_2, but readily etch pits to reveal the extent of dislocation activity. The soft impresser technique has been used to cyclically load (0 0 1), (1 1 0) and (1 1 1) CaF_2 planes for up to 10^6 cycles. The dislocation patterns on the surfaces have been explained in terms of the relevant surface stress contours, derived from elasticity theory. It has been determined that a resolved shear stress of 17 ± 1 MPa is required to initiate dislocation motion for small numbers of cycles, ≤100. However, for high numbers of cycles (≥ 10^5), the stress required to continue dislocation motion decreased to 7 ± 1 MPa.
© 1996 Elsevier Science Limited.

La fatigue de surface est l'un des principaux mécanismes d'usure des matériaux et, de ce fait, de toute première importance pour les céramiques qui sont grandement utilisées pour leur résistance à l'usure. L'objet du présent travail est d'élaborer une approche générale pour l'analyse de la fatigue de surface induite par déformation plastique dans les céramiques. CaF_2 a été choisi comme matériau modèle car il présente la même structure que celle de ZrO_2, commercialement plus important, mais il peut aisément être attaqué chimiquement afin de révéler l'étendue de l'activité des dislocations. La méthode d'impression par cône mou a été employée pour charger cycliquement (de 10 à 10^6 cycles) les plans (0 0 1), (1 1 0) et (1 1 1) de la fluorine. Les motifs des figures d'attaque révélés à la surface ont été expliqués à l'aide de contours d'iso-contraintes obtenus par la théorie de l'élasticité. Pour un faible nombre de cycles (≤ 100), on a montré qu'une contrainte de glissement de 17 ± 1 MPa est nécessaire pour initier le déplacement des dislocations. Cependant, pour un plus grand nombre de cycles (≥ 10^5), la contrainte nécessaire pour continuer la propagation de ces dislocations est réduite à 7 ± 1 MPa.

1 Introduction

In recent years, the field of ceramic fatigue has received increasing attention (see, for example, Refs 1 and 2). A variety of different techniques have been used to generate data on the number of cycles to failure for a given cyclic stress amplitude, i.e. S–N curves, and fatigue crack growth rate as a function of cyclic stress intensity amplitude, i.e. da/dN versus ΔK, for various ceramics. These studies have been useful in demonstrating that true cyclic fatigue does occur in ceramics at low temperatures. However, by analogy with low cycle fatigue in metals, it might be expected that the rate of damage accumulation by cyclic plastic deformation is the dominant phase for fatigue fracture under typical operational conditions.

The study of deformation processes in ceramics is experimentally considerably more difficult than for metals, due to their propensity for brittle fracture. Consequently, hardness testing has been the most used technique for studying monotonic plastic deformation in ceramics. It has been used as a means of identifying slip systems[3] and an indentation technique has been developed to investigate fatigue behaviour.[4] However, a harder indenter necessarily produces substantial immediate localized plasticity which renders this latter approach of limited use for studying plastic deformation in fatigue, as opposed to fatigue crack propagation.

Cyclic fatigue deformation at room temperature in ceramics has received virtually no attention. Thus a new technique has been developed to enable the cyclic deformation processes preceding

fatigue fracture to be studied.[5–7] This method uses a softer material to cyclically impress a ceramic surface. Hence, this induces controlled plastic deformation, the extension of which can be studied with increasing number of cycles. This paper presents an analysis, using classical elasticity theory, to outline the shear stress distribution for this geometry with respect to {0 0 1} <1 1 0> slip. Single-crystal calcium fluoride (CaF_2) has been used as a model ceramic substrate, since it deforms by {0 0 1} <1 1 0> slip at room temperature and can be reliably etch-pitted to reveal the dislocation patterns. The results of the stress analysis have been used to determine values for the critical resolved shear stress, which are comparable with results of Muñoz *et al.* from compression tests.[8] The effect of fatigue on the stress needed to move the dislocations has also been quantitatively assessed. It would be expected that the commercially more important cubic (and possibly tetragonal) zirconias, which are isostructural with CaF_2, would have similar deformation behaviour.

2 Experimental Procedures

2.1 Material

Commercial (Merck Ltd, UK) calcium fluoride single-crystal specimens were employed. These CaF_2 crystals were cleaved on (1 1 1) planes at room temperature. Specimens with (1 1 0) and (0 0 1) faces were obtained by diamond saw cutting followed by grinding using 600 grit water-based SiC slurry on a cast iron wheel. The orientations of the planes were checked to be within ± 2° of the nominal orientation using Laue X-ray back reflection. Chemical polishing of the surfaces proved ineffective and thus all three planes, i.e. (0 0 1), (1 1 0) and (1 1 1), were mechanically polished using 6, 3 and 1/4 μm diamond-paste-impregnated cloths.

The Knoop hardness in the [1 $\bar{1}$ 0] direction in the (1 1 1) plane was measured to be 1·7 GPa, with a load of 0·25 N, and 1·5 GPa, with a load of 4·91 N. These hardness values are slightly lower (~ 5%) than those reported by previous workers.[9,10] It has been shown that the hardness of CaF_2 is not very anisotropic in the (0 0 1), (1 1 0) and (1 1 1) planes, i.e. less than 15%.[9,10]

2.2 Cyclic loading technique and test procedure

The surface fatigue tests were performed in air at room temperature on a purpose-built machine described in detail elsewhere.[5] Using this technique, results have been successfully obtained on various ceramics, e.g. single-crystal magnesium oxide (MgO), ceria-stabilized polycrystalline tetragonal zirconia (Ce-TZP), magnesia partially stabilized zirconia (Mg-PSZ) and calcia-stabilized single-crystal cubic zirconia (Ca-CSZ). True cyclic fatigue could be traced as the cause of the materials' degradation.[5–7]

The technique involves inducing deformation by repeated cyclic point loading of a ceramic substrate using a 120° metallic conical impresser. The fatigue effect is produced by sinusoidally varying the applied load at a frequency of about 2 Hz. The softer cone is flattened to a conforming circular surface on first application of the maximum load and remains in contact with the ceramic surface during the entire duration of the test. Unlike a harder indenter, the softer impresser does not produce immediate gross plastic deformation of the ceramic. The deformation of the cone also ensures a regular pressure distribution.

The metallic impressers were machined from 12 mm diameter round bar magnesinum- and silicon-containing aluminium alloy (BS1474:1972). The tips were subsequently ground to a sharp apical angle of 120°. They were examined in profile under an optical microscope, in order to ensure integrity and sharpness, and cleaned in acetone prior to testing. The Knoop hardness was 1·2 GPa (applied load 0·25 N) before the tests, but increased to 1·5 GPa on the deformed tip, due to work-hardening during cyclic testing.

A load cell was used to output the maximum, minimum and mean loads applied for each cycle, which were recorded via an analogue/digital card to a personal computer. The test range varied between 10 cycles and 10^6 cycles. The cyclic load conditions applied were 9·8 ± 4·9 N, resulting in an applied pressure of 0.56 ± 0·28 GPa over the circular contact area.

3 Stress Analysis

This section is concerned with extending the general results, contained in Johnson,[11] for the elastic analysis of a substrate subjected to a uniform pressure over a circular area, to consider the resolved shear stresses acting on the {0 0 1} <1 1 0> slip systems.

3.1 General analysis

3.1.1 Stress distribution caused by the cone at the surface of the substrate

Elasticity theory can be used to obtain the stress distribution caused by the loading of the deformed cone on the ceramic substrate. The experimental conditions have been designed to ensure that the pressure under the flattened cone is uniform. The

stresses on the surface of the substrate caused by uniform pressure, p, acting on a circular area, radius a, are given by Johnson.[11] Within the contact area, the stress components are all compressive

$$\begin{cases} \sigma_r = \sigma_\theta = -\dfrac{1+2\nu}{2}p \\ \sigma_z = -p \end{cases}$$

where ν is the Poisson's ratio.

Outside the contact area the radial and circumferential stresses are of equal magnitude and are tensile and compressive respectively,

$$\begin{cases} \sigma_r = -\sigma_\theta = \dfrac{1-2\nu}{2}\dfrac{a^2}{r^2}p \\ \sigma_z = 0 \end{cases}$$

where r is the distance from the centre of the circular area to the point where the stresses are defined. For both cases, i.e. inside and outside the contact area, the stresses at the surface σ_r, σ_θ and σ_z are principal stresses.

3.1.2 Stresses acting on slip plane (S)

Let β denote the angle between the test plane (P) and the slip plane (S) (see Fig. 1). In the ($\mathbf{e}_r$, $\mathbf{e}_\theta$, $\mathbf{e}_z$) coordinate system, the normal unit vector to (S) is

$$\mathbf{N} \begin{vmatrix} \sin\beta\cos\alpha \\ \sin\beta\sin\alpha \\ \cos\beta \end{vmatrix}$$

where α is the angle between $\mathbf{e}_r$ and the projection $\mathbf{N}_P$ of $\mathbf{N}$ on (P). Hence, the resultant stress acting on (S) is

$$\boldsymbol{\sigma}_S \begin{vmatrix} \sin\beta\cos\alpha\,\sigma_r \\ \sin\beta\sin\alpha\,\sigma_\theta \\ \cos\beta\,\sigma_z \end{vmatrix}$$

The magnitudes of the normal, σ_{SN}, and shear, σ_{SS}, components of $\boldsymbol{\sigma}_S$ can be calculated inside and outside the contact area using the stress distributions defined in Section 3.1.1:

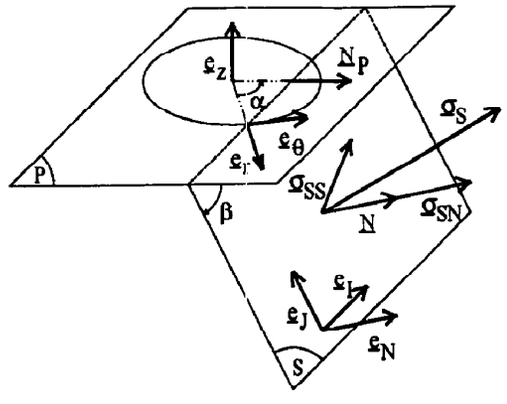

Fig. 1. Schematic diagram presenting the configuration and notations used in the stress analysis.

$$\sigma_{SN} \begin{cases} \text{inside: } \sigma_r \sin^2\beta + \sigma_z \cos^2\beta \\ \text{outside: } \sigma_r \sin^2\beta \cos 2\alpha \end{cases}$$

$$\sigma_{SS} \begin{cases} \text{inside: } (\sigma_r - \sigma_z)\sin\beta\cos\beta \\ \text{outside: } \sigma_r \sin\beta\sqrt{1 - \sin^2\beta\cos^2 2\alpha} \\ \qquad = \sigma_r \sin\beta\cos\beta\sqrt{1 + \tan^2\beta\sin^2 2\alpha} \end{cases}$$

$\boldsymbol{\sigma}_{SS}$ lies in the plane defined by $\mathbf{N}$ and $\boldsymbol{\sigma}_S$, i.e. it is perpendicular to the normal vector $\mathbf{N} \wedge \boldsymbol{\sigma}_s$ of this plane. $\boldsymbol{\sigma}_{SS}$ being also perpendicular to $\mathbf{N}$, its direction is defined by

$$\mathbf{d} = \mathbf{N} \wedge (\mathbf{N} \wedge \boldsymbol{\sigma}_s)$$

that is

$$\mathbf{d} \begin{vmatrix} \sin^3\beta\sin^2\alpha\cos\alpha(\sigma_\theta - \sigma_r) - \cos^2\beta\sin\beta\cos\alpha(\sigma_r - \sigma_z) \\ \cos^2\beta\sin\beta\sin\alpha(\sigma_z - \sigma_\theta) - \sin^3\beta\sin\alpha\cos^2\alpha(\sigma_\theta - \sigma_r) \\ \sin^2\beta\cos\beta\cos^2\alpha(\sigma_r - \sigma_z) - \sin^2\beta\cos\beta\sin^2\alpha(\sigma_z - \sigma_\theta) \end{vmatrix}$$

Considering the stress conditions used here, the expression for $\mathbf{d}$ can be simplified for the inside case as

$$k_1\mathbf{d} \begin{vmatrix} \cos\beta\cos\alpha \\ \cos\beta\sin\alpha \\ -\sin\beta \end{vmatrix}$$

and the outside condition as

$$k_2\mathbf{d} \begin{vmatrix} -\cos\alpha\,(2\sin^2\beta\sin^2\alpha + \cos^2\beta) \\ \sin\alpha\,(2\sin^2\beta\cos^2\alpha + \cos^2\beta) \\ \sin\beta\cos\beta\cos 2\alpha \end{vmatrix}$$

where k_1 and k_2 are constants for given experimental conditions. $\mathbf{d}$ lies in the slip plane (S) and can also be defined by its coordinates d_I and d_J in the ($\mathbf{e}_I$, $\mathbf{e}_J$) system. By definition

$$\mathbf{e}_I \begin{vmatrix} -\sin\alpha \\ \cos\alpha \\ 0 \end{vmatrix} \quad \text{and} \quad \mathbf{e}_J \begin{vmatrix} -\cos\beta\cos\alpha \\ -\cos\beta\sin\alpha \\ \sin\beta \end{vmatrix}$$

For the inside case, $\mathbf{d}$ is equivalent to $\mathbf{e}_J$. For the outside case, comparing the coordinates of $\mathbf{d}$ in both ($\mathbf{e}_r$, $\mathbf{e}_\theta$, $\mathbf{e}_z$) and ($\mathbf{e}_I$, $\mathbf{e}_J$, $\mathbf{e}_N$) systems leads to

$$\begin{cases} -d_I\sin\alpha - d_J\cos\beta\cos\alpha \\ \qquad = -\cos\alpha\,(2\sin^2\beta\sin^2\alpha + \cos^2\beta) \\ d_I\cos\alpha - d_J\cos\beta\sin\alpha \\ \qquad = \sin\alpha\,(2\sin^2\beta\sin^2\alpha + \cos^2\beta) \\ d_J\sin\beta = \sin\beta\cos\beta\cos 2\alpha \end{cases}$$

which simplifies to

$$\begin{cases} d_I = \sin 2\alpha \\ d_J = \cos\beta\cos 2\alpha \end{cases}$$

3.2 Resolved shear stress in CaF_2

At room temperature, the primary slip system of calcium fluoride is {0 0 1} <1 1 0>. The consideration of the three test planes and the possible slip

planes gives rise to three cases, i.e. three values of β, where slip occurs: 45°, 54°44' and 90° (see Tables 1 and 2). Determination of the magnitude and direction of the shear stress in (S) allows calculation of the resolved shear stress, σ_{RSS}, acting on a dislocation. The results for the three test planes, and the possible slip planes, are presented below and summarized in Table 3. When σ_{RSS} is different for the alternative dislocations, only the maximum case is reported.

Table 1. Miller indices for the test plane (P) and slip plane (S) combinations appropriate to this study. β is the angle between (P) and (S), $\mathbf{e}_I$ is defined by the intersection of (P) and (S) and $\mathbf{e}_J$ is orthogonal to $\mathbf{e}_I$ in (S)

Plane (P)	*Plane (S)*	*Direction of e_I*	*Direction of e_J*	β
(0 0 1)	(1 0 0)	[0 1 0]	[0 0 1]	90°
	(0 1 0)	[$\bar{1}$ 0 0]	[0 0 1]	
(1 1 0)	(0 0 1)	[1 $\bar{1}$ 0]	[1 1 0]	90°
	(1 0 0)	[0 0 $\bar{1}$]	[0 1 0]	45°
	(0 1 0)	[0 0 1]	[1 0 0]	
(1 1 1)	(1 0 0)	[0 1 $\bar{1}$]	[0 1 1]	54·74°
	(0 1 0)	[$\bar{1}$ 0 1]	[1 0 1]	
	(0 0 1)	[1 $\bar{1}$ 0]	[1 1 0]	

3.2.1 (0 0 1) test plane

The resolved shear stress on both (1 0 0) and (0 1 0) is zero inside the contact area. Outside the contact area, the angle between **d** and the slip directions, <1 1 0>, is always 45°. Hence

$$\sigma_{RSS} = \frac{1}{\sqrt{2}}\,\sigma_r \sin 2\alpha$$

which is a maximum for $\alpha = 45°$.

3.2.2 (1 1 0) test plane

For the (0 0 1) slip plane, the resolved shear stress is zero inside the contact area while it is the same for both (1 0 0) and (0 1 0) 45° slip planes, i.e.

$$\sigma_{RSS} = \frac{1}{2\sqrt{2}}\,(\sigma_r - \sigma_z)$$

Outside the contact area, the resolved shear stress on (0 0 1) slip plane is zero for [1 1 0] and [$\bar{1}\bar{1}$0] dislocations but is given by

$$\sigma_{RSS} = \sigma_r \sin 2\alpha$$

for [1 $\bar{1}$ 0] and [$\bar{1}$ 1 0] dislocations. For the (1 0 0) and (0 1 0) slip planes, let γ denote the angle between

Table 2. Magnitude and direction of the surface shear stress σ_{SS} in the slip plane (S), inside and outside the contact area for angles β of 90°, 45° and 54·74°

	Inside contact area		*Outside contact area*	
β	σ_{SS}	*d*	σ_{SS}	*d*
90°	0	–	$\sigma_r \sin 2\alpha$	$\mathbf{e}_I$
45°	$\frac{1}{2}(\sigma_r - \sigma_z)$	$\mathbf{e}_J$	$\frac{\sigma_r}{2}\sqrt{1 + \sin^2 2\alpha}$	$\begin{cases} d_I = \sin 2\alpha \\ d_J = \frac{1}{\sqrt{2}}\cos 2\alpha \end{cases}$
54·74°	$\frac{\sqrt{2}}{3}(\sigma_r - \sigma_z)$	$\mathbf{e}_J$	$\frac{\sqrt{2}\sigma_r}{3}\sqrt{1 + 2\sin^2 2\alpha}$	$\begin{cases} d_I = \sin 2\alpha \\ d_J = \frac{1}{\sqrt{3}}\cos 2\alpha \end{cases}$

Table 3. Resolved shear stress σ_{RSS} and polar coordinate r $\{=f(\alpha, \sigma_{RSS})\}$ of the isostress contours outside the contact area for the different test plane (P) and slip plane (S) combinations

Plane (P)	*Plane(S)*	σ_{RSS}	$r = f(\alpha, \sigma_{RSS})$
(0 0 1)	(1 0 0) (0 1 0)	$\frac{1}{\sqrt{2}}\sigma_r \sin 2\alpha$	$r = \left(K\frac{1}{\sqrt{2}}\frac{\sin 2\alpha}{\sigma_{RSS}}\right)^{1/2}$
(1 1 0)	(0 0 1)	$\sigma_r \sin 2\alpha$	$r = \left(K\frac{\sin 2\alpha}{\sigma_{RSS}}\right)^{1/2}$
	(1 0 0) (0 1 0)	$\frac{\sqrt{2}}{4}\sigma_r(\sqrt{2}\sin 2\alpha + \cos 2\alpha)$	$r = \left(K\frac{\sqrt{2}}{4}\frac{(\sqrt{2}\sin 2\alpha + \cos 2\alpha)}{\sigma_{RSS}}\right)^{1/2}$
(1 1 1)	(1 0 0) (0 1 0) (0 0 1)	$\frac{\sqrt{2}}{3}\sigma_r \cos 2\alpha$ $(0° < \alpha < 15°)$	$r = \left(K\frac{\sqrt{2}}{3}\frac{\cos 2\alpha}{\sigma_{RSS}}\right)^{1/2}$
		$\frac{\sqrt{2}}{\sqrt{3}}\sigma_r \sin 2\alpha$ $(15° < \alpha < 45°)$	$r = \left(K\frac{\sqrt{2}}{\sqrt{3}}\frac{\sin 2\alpha}{\sigma_{RSS}}\right)^{1/2}$

$\mathbf{e}_1$ and $\mathbf{d}$. It is also defined by $\tan\gamma = d_J/d_1$. The directions of slip are at 45° from $\mathbf{e}_1$, hence

$$\sigma_{RSS} = \cos\left(\frac{\pi}{4} - \gamma\right)\sigma_{SS}$$

for [1 1 0] and [$\bar{1}\,\bar{1}$ 0] slip directions and

$$\sigma_{RSS} = \sin\left(\frac{\pi}{4} - \gamma\right)\sigma_{SS}$$

for [1 $\bar{1}$ 0] and [$\bar{1}$ 1 0] slip directions. Substituting for γ, and d_1 and d_J, in these equations leads to

$$\sigma_{RSS} = \frac{\sqrt{2}}{4}(\sqrt{2}\sin 2\alpha + \cos 2\alpha)\sigma_r$$

and

$$\sigma_{RSS} = \frac{\sqrt{2}}{4}(\sqrt{2}\sin 2\alpha - \cos 2\alpha)\sigma_r$$

For the first case, σ_{RSS} reaches its maximum $(\sqrt{6}/4)\sigma_r$ for $\alpha = 27{\cdot}36°$.

3.2.3 (1 1 1) test plane

Inside the contact area, the resolved shear stress for the (0 0 1) slip plane is

$$\sigma_{RSS} = \frac{\sqrt{2}}{3}(\sigma_r - \sigma_z)$$

for [1 1 0] and [$\bar{1}\,\bar{1}$ 0] dislocations and zero for [1 $\bar{1}$ 0] and [$\bar{1}$ 1 0] dislocations. The results are similar for (1 0 0) and (0 1 0) slip planes.

Outside the contact area, the shear stress is

$$\sigma_{SS} = \frac{\sqrt{2}\,\sigma_r}{3}\sqrt{1 + 2\sin^2 2\alpha}$$

which is a maximum for $\alpha = 45°$. In the latter case, $\mathbf{d}$ is along $\mathbf{e}_1$ and the maximum resolved shear stress is

$$\sigma_{RSS} = \frac{\sqrt{2}}{\sqrt{3}}\sigma_r$$

on <1 $\bar{1}$ 0> dislocations (but zero on <1 1 0> dislocations) for (0 0 1) slip.

For the general case, consider the (0 0 1) slip plane, the results being similar for the two other planes. If γ denotes the angle between $\mathbf{e}_1$ and $\mathbf{d}$, the resolved shear stress on [1 $\bar{1}$ 0] and [$\bar{1}$ 1 0] dislocations is

$$\sigma_{RSS} = \cos\gamma\,\sigma_{SS} = \frac{\sqrt{2}}{\sqrt{3}}\sigma_r \sin 2\alpha$$

while it is

$$\sigma_{RSS} = \sin\gamma\,\sigma_{SS} = \frac{\sqrt{2}}{3}\sigma_r \cos 2\alpha$$

on [1 1 0] and [$\bar{1}\,\bar{1}$ 0] dislocations. The first value is greater than the second for $0° < \alpha < 15°$ but less for $15° < \alpha < 45°$.

3.3 Isostress resolved shear stress curves for crystals with {0 0 1} <1 1 0> slip system

Considering the analysis outside the contact area, the resolved shear stress is in all cases a function of the angle α and the stress σ_r. Since σ_r is itself a function of the polar coordinate r, it is possible to obtain r as a function of α and σ_{RSS}. If the results are plotted as polar curves for various constant σ_{RSS}, isostress resolved shear stress curves around the contact area are obtained.

Table 3 gives r as a function of α and σ_{RSS} for the various test plane and slip plane combinations. K is a constant equal to $[(1 - 2\nu)/2\pi]L$, where L is the applied load.

The isostress curves, which are calculated using the equations in Table 3, are plotted in Figs 2(a)–(c) for the (0 0 1), (1 1 0) and (1 1 1) planes respectively (for $\nu = 0{\cdot}25$ and $L = 10$ N). These curves are independent of the contact radius, a, but will only apply for $r > a$. On the (0 0 1) test plane, Fig. 2(a), for a given slip plane, the isostress curves have four symmetrical lobes, which would be expected to relate to the extent of dislocation motion in the appropriate directions. These curves all come to a point at the origin, but the equations, and hence plots, do not apply for $r < a$. The lobes however would be expected to extend beyond the contact area, with relative difference illustrated for three arbitrary stress values. Also, in this case, for the two active slip planes, projections of the slip plane normals on the test plane (i.e. N_p) are perpendicular, and hence the isostress patterns superpose. The situation for the (1 1 0) test plane, Fig. 2(b), is somewhat more complex. The (1 0 0) slip plane, which is at 45° to the surface, gives rise to a pattern with eight lobes equidistant from the centre (but with only fourfold symmetry). This curve has four minima, which are 24% closer to the centre than the maxima, and four intermediate minima, at 45° to these. The pattern for the (0 1 0) plane is identical. The (0 0 1) slip plane produces an isostress curve which has the same form as those on (0 0 1) test plane, but the relative magnitude is 1·2 times greater. Again the central part of the curve, i.e. for $r < a$, would not be valid. The isostress pattern for the (1 1 1) plane requires careful consideration. For the (0 0 1) slip plane, there are four large lobes with four smaller intermediate lobes. In this case, these lobes would correspond to the isostress curves for the two different slip directions. The smaller lobes (for $0° \leq \alpha \leq 15°$) represent the shear stress in the [1 1 0] direction and its opposite sense, i.e. [$\bar{1}\,\bar{1}$ 0]. The larger lobes (for $15° \leq \alpha \leq 45°$) correspond to the shear stress in the [1 $\bar{1}$ 0] (and [$\bar{1}$ 1 0]) direction. Equivalent isostress curves are obtained for (1 0 0) and (0 1 0) slip planes with rotations of ± 120° with respect to that for (0 0 1).

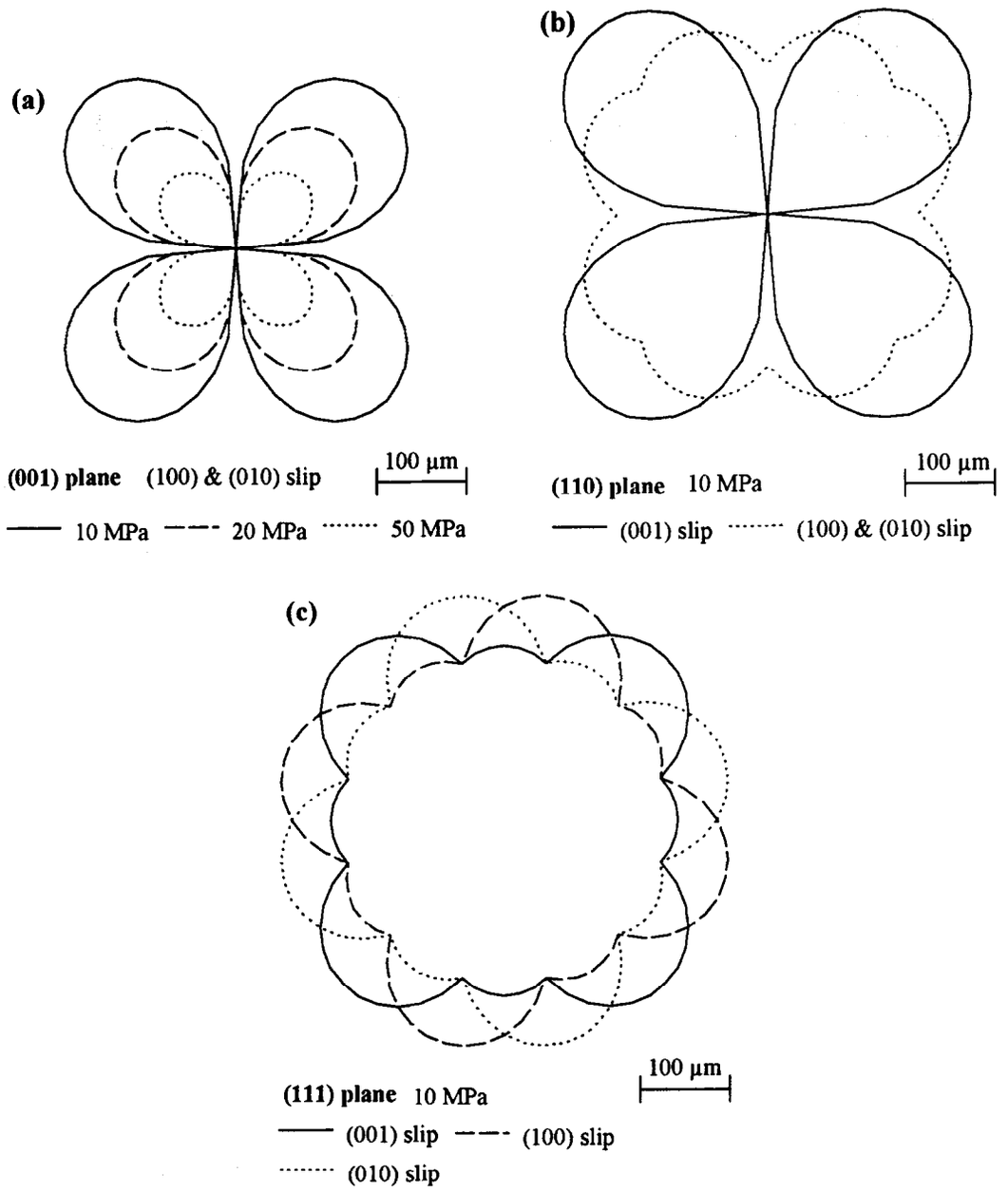

Fig. 2. Isostress resolved shear stress curves for crystals with {0 0 1} <1 1 0> slip system on (a) (0 0 1) plane for isostress values of 10, 20 and 50 MPa, (b) (1 1 0) plane, isostress = 10 MPa and (c) (1 1 1) plane, isostress = 10 MPa. The notional load L is 10 N, resulting in a uniform pressure over a small circular contact area.

4 Experimental Results

4.1 Observations

A new metallic cone was used for each test. The diameters of the tips of the flattened cones were measured afterwards and it was observed that these diameters increased slightly with increasing cycles, i.e. ~8% between 10 and 10^6 cycles on all planes. There was no transfer of material between the cones and CaF_2 substrate. The fatigue contact zone was visible optically in all cases. A cross-sectional depth profile was obtained using a confocal laser scanning microscope, for one test [(1 1 1) test plane, 10^6 cycles], which showed that a shallow, ~4 μm, smooth impression was formed. After the fatigue testing, some cracking in the region adjacent to the contact zone was sometimes observed for the tests at high numbers of cycles, e.g 10^5 on (0 0 1). The CaF_2 specimens were subsequently etched in 20% hydrochloric acid at 70°C and observed by scanning electron microscopy. The etching process induced cracking within or at the edge of the contact zone for (0 0 1) and (1 1 0). Micrographs showing the typical dislocation pattern around the contact area on the (0 0 1) plane are reproduced in Figs 3(a)–(d). The dislocation lines along [1 0 0] and [0 1 0] are due to slip on (0 1 0) and (1 0 0) respectively. It can be observed that the dislocation rosette develops with number of cycles. It becomes denser and the dislocations are moved further away from the contact area at higher number of cycles. After 10^5 cycles the pattern is fully

extended and reaches its limit. Figure 3(e) shows the fully developed dislocation rosette around the contact area on the (1 1 0) plane after 10^5 cycles. The dislocation lines along [1 $\bar{1}$ 0] correlate with (0 0 1) slip while those along [0 0 1] are due to slip on either (1 0 0) or (0 1 0) planes. Slip on all three planes commences at low number of cycles, < 10, which is not the same as observed for similar fatigue tests on MgO.[5] In CaF_2, for a given test condition on the (1 1 0) plane, the resolved shear stresses and the (0 0 1) and (1 0 0)/(0 1 0) planes are similar in magnitude, cf. Fig. 2(b), hence slip on all three planes would be expected. The dislocation pattern after 10^5 cycles around the contact zone on the (1 1 1) plane is shown in Fig. 3(f). The triangular shape, with edge along <1 $\bar{1}$ 0>, is consistent with slip on all three cube planes, i.e. (0 0 1), (0 1 0) and (1 0 1). There is a smaller inverted triangle

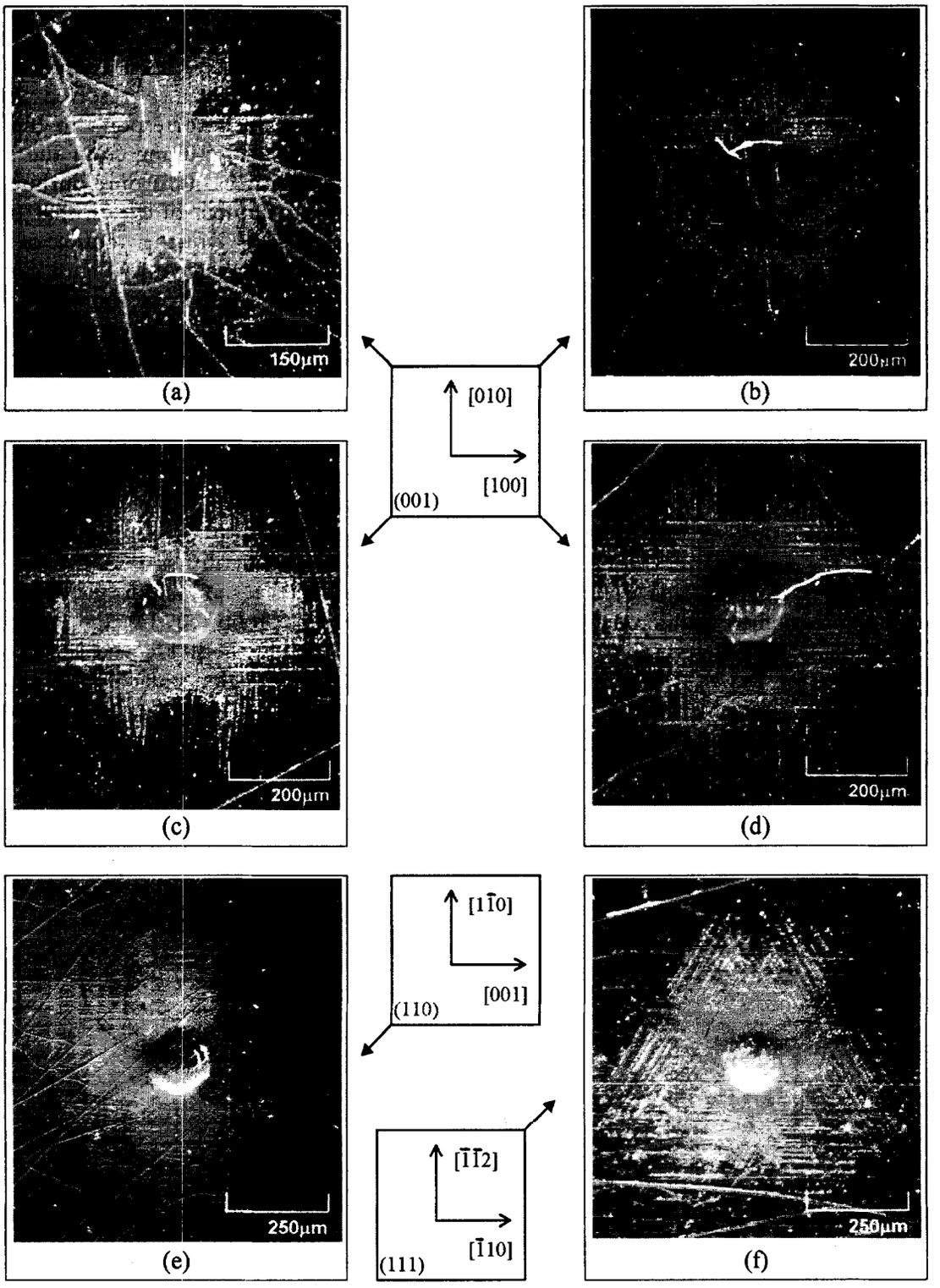

Fig. 3. SEM micrographs of CaF_2 impressed with softer aluminium alloy cones for 9·8 ± 4·9 N cyclic load conditions. Dislocation rosettes around the contact areas on (0 0 1) after (a) 10^2 cycles, (b) 10^3 cycles, (c) 10^4 cycles, (d) 10^5 cycles, (e) on (1 1 0) after 10^5 cycles and (f) on (1 1 1) after 10^5 cycles.

apparent that produces a non-symmetrical 'star of David' shape, which is similar to that observed for Vickers indentations on the (1 1 1) plane of zirconia.[12] Thus it is probable that the slip geometry is similar to that determined by Farber *et al.*,[12] i.e. the larger triangle corresponds to slip on {0 0 1} planes angled towards the contact zone, whereas the smaller one is due to the planes angled away from the contact zone.

4.2 Analysis

4.2.1 Critical resolved shear stress fatigue curve

The isostress curve containing the entire etch pit rosette around the impression can be considered as the limit of dislocation propagation. This can be used to provide an estimate of the critical resolved shear stress in fatigue (CRSSF) of CaF_2 for a specific number of cycles. It was found that the most appropriate method to determine the numerical value of CRSSF was to overlay a net, similar in shape to those in Figs 2(a)–(c), depending on the test plane, but geometrically scaled to the magnifications in Fig. 3, and with isostress contours at 1 MPa intervals. The CRSSF was taken to be the value of isostress (with maximum load L = 14·7 N and ν = 0·23) for the scaled contour which completely encompassed the dislocation rosette. The evolution of the CRSSF with number of cycles for tests on the (0 0 1) plane is presented in Fig. 4. There is some experimental scatter, but discrimination to within ± 1 MPa was found to be possible. For tests on (0 0 1), the CRSSF is ~16 MPa for less than 100 cycles and subsequently decreases to ~7 MPa after 10^5 cycles when the extension of the rosette has effectively stopped. By analogy with conventional fatigue testing, this latter value can be defined as the critical resolved shear stress fatigue limit, CRSSFL.

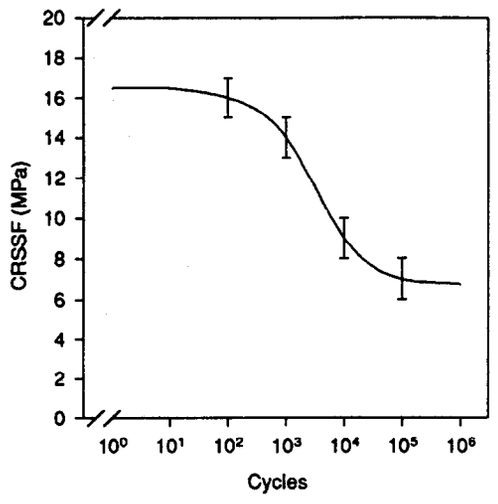

Fig. 4. Critical resolved shear stress in fatigue (CRSSF) versus number of cycles for tests on the (0 0 1) plane. The errors bars are ± 1 MPa.

The dislocation rosette is also fully developed on (1 1 0) and (1 1 1) planes after 10^5 cycles and the estimates of the CRSSFL are ~7 and ~8 MPa, respectively.

4.2.2 Additional critical resolved shear stress estimation method

Figure 4 shows that the resolved shear stress necessary to move dislocations decreases with number of cycles. During an initial phase, up to ~100 cycles, this value is approximately constant and would suggest that it corresponds to the initiation of plastic deformation. This is comparable to the conventional uniaxial critical resolved shear stress measurements, which correspond to the onset of plastic deformation resulting from the activation of dislocation sources. It is only during a second stage, at higher number of cycles, that the rosette expands as a result of further motion of the dislocations generated in stage one. Figure 5 represents the isostress curves for the initial deformation phase, I, and the maximum extent of the dislocation motion at the end of phase II. It can be postulated therefore that dislocations will be generated within zone I, and then these dislocations are able to move further outwards to a limit defined by zone II. The dashed lines thus schematically represent the resultant expected dislocation pattern. This can be compared with Figs 3(a) and (d) which demonstrate an initially square array of dislocation etch pits, corresponding to phase I [Fig. 3(a)], which then is followed by the formation of extended wings in the [0 1 0] and [1 0 0] directions at the corners of the square array [Fig. 3(d)]. There is no expansion of the dislocation array in the [0 1 0] or <1 1 0> directions, as would be predicted from consideration of Fig. 5. There is,

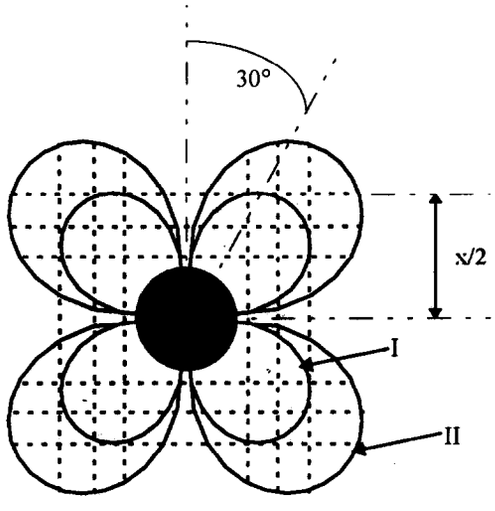

Fig. 5. Schematic diagram of isostress contours and corresponding dislocation rosette around the contact area on the (0 0 1) plane. The inner isostress contour, I, corresponds to the initial dislocation generation and motion stage. The outer isostress contour, II, represents the limit of the subsequent propagation of these dislocations by fatigue.

however, an observed extension of the dislocation array in the [1 0 0] direction, which would not be expected on the basis of the present model. The dimension of the square etch pit array enables a value of the CRSS to be estimated. It is only necessary to determine the isostress corresponding to curve I in Fig. 5. The dislocation array will be a tangent to the isostress curve at $\alpha = 30°$, and thus measurement of x (see Fig. 5) enables r to be determined since $r = (x/2)(1/\cos\alpha)$. The CRSS can then be calculated as the stress defined by the appropriate formula in Table 3. A restriction of this particular approach is that it can only be applied to slip on planes perpendicular to the tested surface. From Figs 3(d) and (e) the values of x corresponding to the 90° slip planes are 360 and 440 μm, respectively. From these, the CRSS is estimated to be 17·9 and 17·0 MPa, respectively.

5 Discussion

The present work shows that CaF_2 is susceptible to fatigue under cyclic point loading conditions. The plastic deformation caused by pressing a softer cone onto the surface increases with number of cycles as shown by the dislocation rosettes in Figs 3(a)–(d). Similar observations have been reported by Guillou *et al.* on MgO.[5] The etched CaF_2 surfaces present etch pit patterns around the impressions on the (0 0 1), (1 1 0) and (1 1 1) planes that are consistent with {0 0 1} <1 1 0> slip. Muñoz *et al.* have recently confirmed this slip system to be the primary one at room temperature by performing compression tests in various orientations.[8] They also observed that slip on {1 1 1} was obtained only above 90°C when {0 0 1} slip could not be activated. It is possible that, in the present work, {1 1 1} slip may be responsible for plastic deformation inside the contact area on the (0 0 1) plane when the {0 0 1} <1 1 0> slip system is not active, i.e. $\sigma_{SS} = 0$ (see Table 2).

As discussed in Section 4.2.2, it is proposed that significant dislocation motion may occur under cyclic loading conditions at stresses less than the critical resolved shear stress. As described above, the CRSS can be estimated using elastic stress analysis as ~16 MPa on (0 0 1) (Fig. 4, Section 4.2.1) or 17·9 and 17·0 MPa on (0 0 1) and (1 1 0), respectively (Section 4.2.2). The presence of plastic deformation will obviously result in the stress distribution being different from that predicted by linear elasticity theory. It would be expected that this difference would possibly be considerable in the central region, where there is extensive plasticity, but of much less significance at the boundary between the elastic and plastic zones. The initial results of a finite element analysis[13] confirm that the stress at the edge of the contact zone may be significantly modified as a result of plastic deformation, but the discrepancy between the plastic and elastic–plastic values for σ_r decreases rapidly as r increases beyond the contact zone. Experimental support for the use of the elastic stress distributions is provided by the results of Muñoz *et al.*,[8] who determined a value of 15 MPa for the CRSS in CaF_2; this is close to those estimated in the present study, i.e. 17 ± 1 MPa. Thus, it can be assumed that the values of critical resolved shear stress in fatigue (Fig. 4) derived from the elastic stress distributions are reasonably accurate estimates. The limiting value for the critical resolved shear stress in fatigue, CRSSFL, has been estimated as 7 ± 1 MPa for all three test planes, (Section 4.2.1). The ratio between the CRSSFL and the monotonic CRSS, i.e. ~0·4, is comparable to the ratio of fatigue limits to static strengths obtained in metallic alloys, i.e. ~0·3–0·5,[14,15] which occurs as a result of the dislocation substructures formed during fatigue. This similarity supports the interpretation presented herein for both the shapes of the etch pit patterns, and their evolution with increasing number of cycles, resulting from an initial dislocation generation phase followed by propagation of these dislocations at lower cyclic stresses, and the use of linear elasticity to determine the respective critical resolved shear stress.

Brookes and co-workers[16,17] have used a static soft impresser method to estimate the CRSS in MgO, but the analytical approach was substantially different. In their approach, different contact pressures were applied to the surface by using impressers of different hardnesses. Subject to several assumptions concerning the geometry of the dislocation motion, the CRSS was estimated from the minimum contact pressure required to develop dislocations beneath the contact area. The analysis presented in this paper provides an alternative approach that does not require as many tests, nor such precise matching of the relative hardnesses of the substrate and impresser.

6 Conclusions

The test procedure used in this paper relies upon a flat ceramic substrate being subjected to a contact pressure as a result of loading via a softer, initially conical, impresser. This geometry is also eminently suitable for cyclical loading. An analysis of the shear stresses on the {0 0 1} <1 1 0> slip system for (0 0 1), (1 1 0) and (1 1 1) test planes has been presented.

Plastic deformation in single-crystal calcium fluoride was achieved under conditions of repeated cyclic loading with a softer impresser, i.e. an aluminium alloy cone (relative hardnesses 1·7 and 1·2 GPa, respectively), on (0 0 1), (1 1 0) and (1 1 1) test planes. The extent of the plastic deformation was revealed using etch pitting of the dislocations. This showed that the plastic zone around the circular contact area increased with number of cycles to a maximum size at about 10^5 cycles. A comparison of the calculated surface isostress resolved shear stress contours with observed size and shape of the dislocation arrays enabled estimates to be made of the critical resolved shear stress and critical resolved shear stress fatigue limit (CRSSFL) of 17 ± 1 and 7 ± 1 MPa, respectively. The value for the CRSS is consistent with the findings of other workers[8] and the CRSS:CRSSFL ratio of ~0·4 lies within the equivalent range of static: fatigue strengths for metallic systems (0·3–0·5).

Acknowledgement

The authors would like to thank Mr Koremura of Lasertec Corporation (London) for the confocal laser scanning microscopy.

References

1. Ritchie, R. O., Dauskardt, R. H. & Cox, B. N., *Fatigue of Advanced Materials.* Proceedings of the Engineering Foundation, International Conference, Santa Barbara, CA, 1991.
2. Kishimoto, H., Hishide, T. & Okabe, N., *Cyclic Fatigue in Ceramics.* Elsevier Science BV & The Society of Materials-Japan, 1995.
3. Brookes, C. A., O'Neill, J. B. & Redfern, B. A. W., Anisotropy in the hardness of single crystals. *Proc. Roy. Soc. Lond. A*, **322** (1971) 73–88.
4. Vaughan, D. A. J., Guiu, F. & Dalmau, M. R., Indentation fatigue of alumina. *J. Mater. Sci. Lett.*, **6** (1987) 689–691.
5. Guillou, M.-O., Henshall, J. L. & Hooper, R. M., Indentation cyclic fatigue of single-crystal magnesium oxide. *J. Am. Ceram. Soc.*, **76** [7] (1993) 1832–1836.
6. Guillou, M.-O., Henshall, J. L. & Hooper, R. M., Surface fatigue in ceria-stabilized polycrystalline tetragonal zirconia between room temperature and 1073K. *J. Mater. Sci.*, **30** (1995) 151–161.
7. Henshall, J. L., Guillou, M.-O. & Hooper, R. M., Point contact surface fatigue in zirconia ceramics. *Trib. Int.*, **28** (1995) 363–376.
8. Muñoz, A., Domínguez-Rodríguez, A. & Castaing, J., Slip systems and plastic anisotropy in CaF_2. *J. Mater. Sci.*, **29** (1994) 6207–6211.
9. O'Neill, J. B., Redfern, B. A. W. & Brookes, C. A., Anisotropy in the hardness and friction of calcium fluoride crystals. *J. Mater. Sci.*, **8** (1973) 47–58.
10. Burnand, R. P., Zone refining of carbides and the hardness of crystals. PhD thesis, University of Exeter, UK, 1974.
11. Johnson, K. L., *Contact Mechanics.* Cambridge University Press, Cambridge, 1985.
12. Farber, B. Y., Chiarelli, A. S. & Heuer, A. H., A dislocation mechanism of crack nucleation in cubic zirconia single crystals. *Phil. Mag. A*, **70** [1] (1994) 201–217.
13. Dupas, F., Finite element analysis of an indentation. MEng (Eur) thesis, University of Exeter, UK, 1994.
14. Kettunen, P., S–N curves of copper single crystals. *Phil. Mag.*, **14** (1966) 421–426.
15. Hertzberg, R. W., *Deformation and Fracture Mechanics of Engineering Materials.* John Wiley & Sons, 1976.
16. Shaw, M. P. & Brookes, C.A., Dislocations produced in magnesium oxide crystals due to contact pressures developed by softer cones. *J. Mater. Sci.*, **24** (1989) 2727–2734.
17. Brookes, C. A., Brookes, E. J., Howes, V. R., Roberts, S.G. & Waddington, C. P., A comparison of the plastic deformation and creep of type I, type II and synthetic diamonds at 1100°C under conditions of point loading. *J. Hard Mater.*, **1** (1990) 3–24.